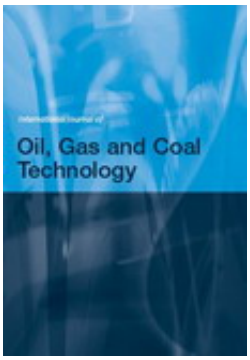

International Journal of Oil, Gas and Coal Technology

ISSN online: 1753-3317 - ISSN print: 1753-3309
https://www.inderscience.com/ijogct

Study on gas-water-sand-hydrate foam flow and discharge in the wellbore during hydrate depressurisation production

Haitao Li, Xuefei Zhang, Na Wei, Jianyong Feng, Zhaolong Ge, Shuning Yi, Liehui Zhang, Bjørn Kvamme, Richard Banks Coffin

DOI: 10.1504/IJOGCT.2025.10073241

Article History:

Received:	06 May 2025
Last revised:	03 July 2025
Accepted:	08 July 2025
Published online:	31 March 2026

Study on gas-water-sand-hydrate foam flow and discharge in the wellbore during hydrate depressurisation production

Haitao Li

State Key Laboratory of Oil and Gas
Reservoir Geology and Exploitation,
Southwest Petroleum University,
Xindu Road No. 8, Chengdu 610500, China
Email: 201799010071@swpu.edu.cn
and
State Key Laboratory of Coal Mine Disaster Dynamics and Control,
Chongqing University,
Chongqing, 400044, China

Xuefei Zhang*

State Key Laboratory of Oil and Gas
Reservoir Geology and Exploitation,
Southwest Petroleum University,
Xindu Road No. 8, Chengdu 610500, China
Email: 202321000882@stu.swpu.edu.cn
*Corresponding author

Na Wei and Jianyong Feng

State Key Laboratory of Oil and Gas
Reservoir Geology and Exploitation,
Southwest Petroleum University,
Xindu Road No. 8, Chengdu 610500, China
Email: weina8081@163.com
Email: 202322000875@stu.swpu.edu.cn

Zhaolong Ge

State Key Laboratory of Coal Mine
Disaster Dynamics and Control,
Chongqing University,
Chongqing, 400044, China
Email: gezhaolong@cqu.edu.cn

Shuning Yi and Liehui Zhang

State Key Laboratory of Oil and Gas
Reservoir Geology and Exploitation,
Southwest Petroleum University,
Xindu Road No. 8, Chengdu 610500, China
Email: 1421675116@qq.com
Email: 19992526256@163.com

Bjørn Kvamme

State Key Laboratory of Oil and Gas
Reservoir Geology and Exploitation,
Southwest Petroleum University,
Xindu Road No. 8, Chengdu 610500, China
and
Department Physics and Technology,
University of Bergen,
Allegaten 55, Bergen, N-5007, Norway
Email: updatesix@yeah.net

Richard Banks Coffin

State Key Laboratory of Oil and Gas
Reservoir Geology and Exploitation,
Southwest Petroleum University,
Xindu Road No. 8, Chengdu 610500, China
and
Department of Physical and Environmental Science,
Texas A&M University – Corpus Christi,
Corpus Christi, TX, 78412, USA
Email: muling947@gmail.com

Abstract: To address sand and water production in hydrate reservoirs that affect the production efficiency, this study innovatively considers the application of foam drainage to hydrate production scenarios. Using a multi-physics field coupling approach, a numerical model of continuous foam drainage in wellbores based on the liquid- and solid-carrying models and other models is developed, and its evaluation accuracy was verified to be up to 95% by comparing with the indoor experimental data. Correlation factor analysis showed that increasing nitrogen injection rate, gas production rate and gas-liquid ratio enhanced liquid and solid transport efficiency. However, both excessive foam viscosity and overly low viscosity adversely affect system performance. Under South China Sea hydrate trial conditions, the study employed model predictions and multi-factor analysis to determine optimal foam injection rates for varying water/sand production levels. The findings provide theoretical guidance for optimising continuous foam drainage technology in hydrate wells, aiding in productivity enhancement. [Received: May 18, 2025; Accepted: July 8, 2025]

Keywords: foam drainage; wellbore fluid accumulation; reservoir sand production; natural gas hydrate; numerical simulation.

Reference to this paper should be made as follows: Li, H., Zhang, X., Wei, N., Feng, J., Ge, Z., Yi, S., Zhang, L., Kvamme, B. and Coffin, R.B. (2026) 'Study on gas-water-sand-hydrate foam flow and discharge in the wellbore during hydrate depressurisation production', *Int. J. Oil, Gas and Coal Technology*, Vol. 39, No. 5, pp.1–29.

Biographical notes: Haitao Li is a Lecturer at Southwest Petroleum University. He is a PhD student at Chongqing University. His current research focuses on natural gas hydrate extraction, pipeline multiphase flow, and oil and gas development

Xuefei Zhang is a current graduate student at Southwest Petroleum University. Her current research focuses on gas lift, gas hydrate extraction, and oil and gas development

Na Wei is a Professor at Southwest Petroleum University. His research focuses on marine natural gas hydrate extraction technology, pressure-controlled drilling, underbalanced drilling, and fluid mechanics.

Jianyong Feng is a current graduate student at Southwest Petroleum University. His current research focuses on CO_2 replacement for natural gas hydrate exploitation, carbon capture and storage, and sand production from hydrate reservoirs.

Zhaolong Ge is a Professor at the School of Resources and Safety Engineering at Chongqing University. His research focuses on the theory and technology of high-pressure water jets, as well as the development of unconventional natural gas.

Shuning Yi is a current graduate student at Southwest Petroleum University. Her current research focuses on gas hydrate extraction and multiphase flow studies.

Liehui Zhang is a Professor at Southwest Petroleum University. His research focuses on the theory of multiphase flow in complex oil and gas reservoirs, well testing, and numerical simulation.

Bjørn Kvamme is a Professor at University of Bergen. His research focuses on CCUS, CO_2 enhanced oil recovery, and geological risk analysis of natural gas hydrate extraction.

Richard Banks Coffin is a Professor at Texas A&M University. His primary areas of study are environmental chemistry, bacteria, dissolved organic carbon, estuary and bacterioplankton.

1 Introduction

With the advancement of technology and the proposal of the 'dual carbon' goals, the global energy landscape is undergoing the 'third major transition' from traditional fossil fuels to new energy sources (Hou et al., 2021). Energy transition is a prolonged and

gradual process, and natural gas, due to its wide distribution, abundant reserves, and clean, low-carbon attributes, is regarded as a crucial transitional energy source during this transformation. It is expected to coexist with low-carbon and zero-carbon energy sources in the long term. Natural gas hydrate, as one of the most resource-rich unconventional natural gas resources yet to be developed, holds immense potential, with proven deposits containing at least 1,013 t carbon content, approximately twice as much as existing fossil energy sources (Zhao et al., 2022; Li et al., 2022). With its high gas storage density, 1 m^3 of hydrate can decompose into 164 m^3 of methane gas and 0.8 m^3 of water under standard conditions (Fu et al., 2015). However, during natural gas hydrate extraction, phase alterations and hydrate decomposition trigger the migration and precipitation of gas and water, consequently leading to water and sand production. These issues have emerged as substantial impediments to the efficient and reliable improvement of natural gas hydrates. In 2002, sand production was first identified as a critical constraint to efficient extraction in the Mallik 5L-38 pilot project (Haberer et al., 2006; Kurihara, 2005; Fujii et al., 2013). To date, in the 12 pilot extraction activities conducted in the former Soviet Union, Canada, the USA, Japan, and China, water and sand production issues have frequently arisen (Shaibu et al., 2021). Notably, in Canada's second pilot extraction in 2007 and Japan's first pilot extraction in 2013, sand production at the well bottom directly led to the suspension of the projects (Yamamoto et al., 2014; Kurihara et al., 2010; Xu, 2022). Therefore, studying appropriate water and sand drainage measures and applying them in hydrate extraction processes is an effective approach to achieving the efficient development of natural gas hydrates. Among several typical drainage techniques, foam drainage, with its simple design, high flexibility, and excellent sand and scale control, is particularly suitable for addressing water and sand production issues in hydrate reservoirs (Zhu, 2020; Boussa, 2004).

Foam drainage technology involves injecting surfactants into the well bottom to induce various physical and chemical effects, such as foaming, dispersion, drag reduction, and cleaning, during the mixed flow of gas and liquid phases. The generated low-density aqueous foam is transported by the gas flow from the well bottom to the surface, thereby removing accumulated liquid and sand in the wellbore. Extensive research has been conducted on foam drainage in conventional oil and gas extraction (Kruglyakov et al., 2008; Koehler et al., 2000; Guo et al., 2023). Stevenson et al. (2007) identified nuclear magnetic resonance imaging (NMRI) as an effective non-invasive method for measuring the drainage rate at the foam surface. They utilised this technique to investigate the spatial and temporal distribution of liquid holdup in foam, revealing that liquid holdup varies cyclically over time but shows no clear pattern along the foam column's axis. Etemad et al. (2022) proposed a generalised version of the drainage equation to predict foam longevity in later stages and established the relationship between foam volume and time. Lai et al. (2022) utilised molecular dynamics simulations to explore the molecular dynamics and interactions of APG foam within diverse gas phase environments, summarising the influence of different gas components on the foam's coarsening process and liquid drainage. Alooghareh et al. (2022) experimentally evaluated foam performance using seven different gases as the gaseous phase and found that a combination of 80% N_2 and 20% CO_2 significantly enhanced oil recovery. On the other hand, Li et al. (2023) investigated the impact of the formation of sand on foam performance through indoor experiments and examined the behaviour of different foam drainage agents in sand-containing conditions. Rahman et al. (2023, 2024) explored the effectiveness of various nanoparticle-surfactant combinations in foam generation for

enhanced oil recovery and focused on the enhancement of CO_2 foam drive by nanoparticles through micro-optical analysis. Jin et al. (2024) observed that particles of intermediate size more significantly increase viscous losses at the plateau border in studies on the influence of particles on foam drainage. Zhang et al. (2024) noted that increased foam viscosity during foam-drainage gas recovery reduces drainage capacity and exacerbates hydrate formation. To expand the application scope of foam drainage technology, considerable research efforts have been directed toward the innovation and refinement of surfactants (Alyousef et al., 2018; Silin et al., 2018; Wu and Guo, 2023). For example, Lai et al. (2023) synthesised a foam drainage agent that is resistant to both temperature and salt, while Ning et al. (2024) developed a cold- and high-temperature-resistant foam drainage agent applicable over a temperature range of 238 to 423 K. Li et al. (2024) developed an innovative surfactant featuring pH-sensitive characteristics to tackle the issue of maintaining equilibrium between foam formation and disintegration in conventional foam-assisted gas recovery operations.

Despite the rapid advancement and widespread adoption of foam-assisted lift, research efforts have predominantly focused on the prediction and enhancement of the effectiveness of foam drainage under conventional oil and gas extraction and developing high-efficiency surfactants. Conventional reservoir foam drainage mainly deals with formation free water and a small amount of intermittently cemented sand particles, while hydrate reservoirs need to continuously carry a large amount of free water and highly viscous muddy sand particles generated by hydrate decomposition. In addition, it is also necessary to prevent the secondary generation of hydrate plugging in the wellbore. Therefore, the application of conventional reservoir foam drainage in hydrate extraction is limited. At present, there is no example of foam drainage that can be effectively applied to the production of marine hydrates, and there are fewer studies on foam drainage after sand release from hydrate reservoirs. Therefore, this paper applies the foam circulation and solid-liquid conveyance process to hydrate reservoirs. And considering the slow decomposition rate of hydrate in the reservoir, the small and slow gas flow into the wellbore, which is difficult to mix the foam drainage agent sufficiently, it is proposed to add the injection pipe in the original tubing. The direct injection of foam drainage agents and gas into the well compensates for the slow rate of hydrate decomposition, ensures full formation of foam, and enhances liquid and solid transportation efficiency. On this basis, a theoretical model is established, and its accuracy is verified through experiments. Subsequently, numerical computations and analyses of the factors influencing multiphase flow within the wellbore are conducted under various conditions, and the optimised design of engineering parameters is carried out based on the actual field data. Compared with the high cost and poor adaptability of traditional mechanical sand control technologies, foam drainage breaks through the traditional ‘sand suppression’ approach by achieving ‘sand-water synergistic diversion’ through multiphase flow regulation. This method better compensates for the limitations of traditional mechanical sand control in argillaceous siltstone reservoirs, reduces pipeline erosion caused by gravel, and achieves the dual objectives of reservoir protection and enhanced production. Offered a methodological reference for addressing issues of water and sand production in hydrate reservoir extraction.

2 Theoretical model

2.1 Model formulation

2.1.1 Continuity equation

Taking a fluid segment of length *dz* as the control volume for the continuity equation, an analysis is conducted for the gas, liquid, and solid phases within the control volume. In the multiphase flow of continuous discharge wellbore, considering the effects of hydrate phase transitions, add the gas-phase mass change q_g and the liquid-phase mass change q_l caused by hydrate phase transition. After integration and simplification, the mathematical theoretical model for continuous multiphase flow within the wellbore [equations (1)–(4)] is derived as follows:

$$\frac{\partial}{\partial t}\left(A\rho_g\alpha_g\right)+\frac{\partial}{\partial z}\left(A\rho_g\alpha_g v_g\right)=q_g \tag{1}$$

$$\frac{\partial}{\partial t}\left(A\rho_l\alpha_l\right)+\frac{\partial}{\partial z}\left(A\rho_l\alpha_l v_l\right)=q_l \tag{2}$$

$$\frac{\partial}{\partial t}\left(\rho_c\alpha_c\right)+\frac{\partial}{\partial z}\left(\rho_c\alpha_c v_c\right)=0 \tag{3}$$

$$\frac{\partial}{\partial t}\left(\rho_h\alpha_h\right)+\frac{\partial}{\partial z}\left(\rho_h\alpha_h v_h\right)=-q_l-q_g \tag{4}$$

Based on the continuum medium theory, there is equation (5):

$$\alpha_g+\alpha_l+\alpha_h+\alpha_c=1 \tag{5}$$

where q_g and q_l are the mass change of the gas phase and the liquid phase caused by hydrate phase transition respectively, kg/m^3; ρ_g, ρ_l, ρ_c and ρ_h are the gas phase density, the liquid phase density, the solid phase density, and the hydrate phase density, kg/m^3; v_g, v_l, v_c and v_h are the gas phase velocity, the liquid phase velocity, the solid phase velocity, and the hydrate phase velocity, m/s; α_g, α_l, α_c and α_h are the gas holding rate, the liquid holding rate, the solid holding rate, and the hydrate holding rate, dimensionless.

2.1.2 Equation of motion

Taking a fluid segment of length dz as the control volume for the equation of motion, let the cross-sectional area of the flow channel be denoted as $A = A(z, t)$, the pressure within the system as $p = p(z, t)$, and the flow rate as $v_g = v_g(z, t)$, then analyse the forces on the gas phase within the control body. In accordance with Newton's second law, the momentum equation for the gas phase within a control volume of a constant cross-sectional flow channel is given by equation (6):

$$\frac{\partial}{\partial t}\left(\rho_g\alpha_g v_g\right)+\frac{\partial}{\partial z}\left(p\alpha_g+\rho_g\alpha_g v_g^2\right)+\rho_g\alpha_g g\sin\theta+\frac{\tau_{wg}S_{wg}}{A}=0 \tag{6}$$

The remaining two-phase momentum equations are identical, and a representation of the shear stress between the mixture and the wall in the form of friction can be seen in equation (7):

$$\frac{\tau_{wg}S_{wg}+\tau_{wl}S_{wl}+\tau_{ws}S_{ws}}{A}=\frac{f\rho_m v_m^2}{2D} \tag{7}$$

By summing the momentum equations for each phase and substituting them into equation (7), the multiphase flow motion equation for a continuously producing wellbore [equation (8)] can be obtained.

$$\begin{aligned}&\frac{\partial}{\partial t}\left(\rho_g\alpha_g v_g+\rho_l\alpha_l v_l+\rho_s\alpha_s v_s\right)+\frac{\partial}{\partial z}\left(p+\rho_g\alpha_g v_g^2+\rho_l\alpha_l v_l^2+\rho_s\alpha_s v_s^2\right)\\&+\left(\rho_g\alpha_g+\rho_l\alpha_l+\rho_s\alpha_s\right)g\sin\theta+\frac{f\rho_m v_m^2}{2D}=0\end{aligned} \tag{8}$$

where p is the pressure in the system, Pa; ρ_m is mixed phase density, kg/m^3; v_m is the mixed phase velocity, m/s; D is the inner diameter of the tube, m; f is the coefficient of friction resistance, dimensionless.

2.1.3 Pressure field model

During the foam drainage process, the foam phase acts as the continuous phase and dominates the flow, while the gas phase is encapsulated as dispersed bubbles. The flow behaviour approximates that of a pseudo-single-phase fluid. The flow direction dominance in the wellbore is clear, and the radial velocity component has less influence, which meets the geometrical premise of one-dimensional flow. Therefore, assuming that the wellbore flow is treated as a steady one-dimensional flow of a single-phase compressible fluid, as illustrated in Figure 1, the pressure gradient equation shown in equation (9) can be obtained:

$$\frac{dp}{dz}=-\left(\rho g\sin\theta+f\frac{\rho v^2}{2D}+\rho v\frac{dv}{dz}\right) \tag{9}$$

$$\frac{dp}{dz}=\left(\frac{dp}{dz}\right)_G+\left(\frac{dp}{dz}\right)_F+\left(\frac{dp}{dz}\right)_A \tag{10}$$

where the direction of fluid flow is represented by the positive value of coordinate z.; p is the pressure, Pa; ρ is the density of fluid, kg/m^3; g is the acceleration of gravity, m/s^2; θ is the pipe inclination, °; v is the velocity of the fluid, m/s; f is coefficient of friction resistance, dimensionless. G, F and A in equation (10) denote the gravitational pressure drop, frictional pressure drop, and kinetic energy pressure drop, respectively.

2.1.4 Temperature field model

Within the system composed of fluids in the wellbore, tubing, casing, cement ring, stratum, and seawater, continuous heat exchange occurs, as illustrated in Figure 2. As a result, the temperature within the tubing undergoes constant variation.

Figure 1 Stabilising one-dimensional gas-phase flow

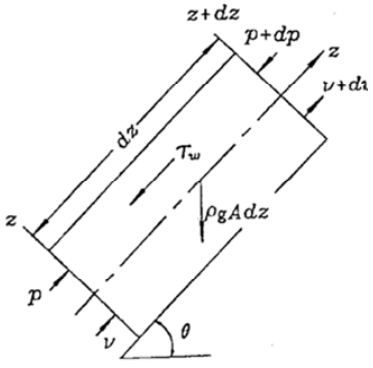

Figure 2 Schematic representation of heat transfer within the wellbore, (a) below the mudline (b) above the mudline (see online version for colours)

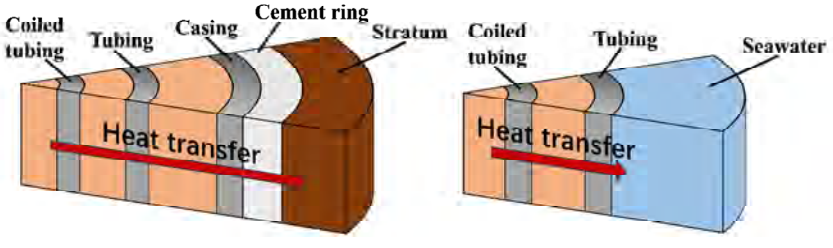

(a) (b)

By incorporating the principles of the law of energy conservation and the fundamental equations of heat conduction (Wei et al., 2017; Li et al., 2019), and referencing the wellbore temperature distribution model established by Wei et al. (2020) for the water-bearing natural gas production process, a temperature field model tailored to the working conditions of this paper is developed as in equation (11).

$$\frac{dT_m}{dz} = \frac{-4}{\rho_m v_m c_m \pi D_{oi}^2}\left(q_f + q_h + q\right) \tag{11}$$

where each of the computational equations [equation (12)–(16)] is:

$$q_f = \frac{2 f v_m^2 \rho_m}{D_{oi}} \times \frac{\pi D_{oi}^2 v_m}{4} \tag{12}$$

$$q_h = \Delta n_{hyd} q_{hyd} \tag{13}$$

$$q = \begin{cases} \dfrac{\pi D_{oi} U_s}{Q_m}\left(T_m - T_s\right), & z > h_w \\ \dfrac{\pi D_{oi} U_w}{Q_m}\left(T_w - T_m\right), & z \le h_w \end{cases} \tag{14}$$

$$U_s = \left[\frac{1}{\alpha_{oi}} + \frac{D_{oi}}{2\lambda_o} \ln\left(\frac{D_{oo}}{D_{oi}}\right) + \frac{D_{oi}}{D_{oc}\alpha_{op}} + \frac{D_{oi}}{2\lambda_p} \ln\left(\frac{D_{po}}{D_{pi}}\right) + \frac{D_{pi}}{D_{pc}\alpha_{pc}} + \frac{D_{oi}}{2\lambda_c} \ln\left(\frac{D_{co}}{D_{ci}}\right) + \frac{D_{oi}}{2\lambda_{cs}} \ln\left(\frac{D_{cso}}{D_{csi}}\right) + \frac{D_{oi}}{2\lambda_s} \ln\left(\frac{D_{so}}{D_{si}}\right) \right]^{-1} \tag{15}$$

$$U_w = \left[\frac{1}{\alpha_{oi}} + \frac{D_{oi}}{2\lambda_o} \ln\left(\frac{D_{oo}}{D_{oi}}\right) + \frac{D_{oi}}{D_{oc}\alpha_{op}} + \frac{D_{oi}}{2\lambda_p} \ln\left(\frac{D_{po}}{D_{pi}}\right) + \frac{D_{pi}}{D_{po}\alpha_{pw}} \right]^{-1} \tag{16}$$

where z is the well depth, m; h_w is the depth of sea, m; ρ_m is the mixed fluid density in the wellbore, kg/m^3; v_m is the mixed fluid velocity in the wellbore, m/s; c_m is the specific heat capacity of the mixed fluid in the wellbore, J/(kg·K); f is coefficient of friction resistance, dimensionless; Δn_{hyd} is the amount of substance undergoing a phase transition in hydrate per unit length per unit time, mol/(s·m); q_{hyd} is the heat of phase transition of hydrates per unit amount of substance, J/mol; T_m, T_s and T_w is the wellbore temperature, formation temperature, and seawater temperature, K; D_{oi}, D_{oo}, D_{pi}, D_{po}, D_{ci}, D_{co}, D_{csi}, D_{cso} and D_s are the inner diameter of coiled tubing, the outer diameter of coiled tubing, the inner diameter of tubing, the outer diameter of tubing, the inner diameter of casing, the outer diameter of casing, the inner diameter of the cement ring, the outer diameter of the cement ring, and the diameters corresponding to the range of temperature action in the formation, respectively, m; D_{oc} and D_{pc} are the equivalent diameters of the annulus between the coiled tubing and the tubing, and the annulus between the outer wall of the tubing and the casing, respectively, m; α_{oi}, α_{op}, α_{pc} and α_{pw} are the convective heat transfer coefficients for the inner wall of the coiled tubing, the annulus between the coiled tubing and the tubing below the mudline, the annulus between the tubing and the casing below the mudline, and the outer wall of the tubing in contact with seawater, respectively, W/(m^2·K); λ_o, λ_p, λ_c, λ_{cs} and λ_s are the thermal conductivities of the tubing, casing, cement ring, and formation, respectively, W/(m·K).

2.1.5 Critical liquid-carrying model

In this paper, the Turner model is used to calculate the critical fluid-carrying capacity (Turner et al., 1969). Turner has adjusted the model coefficients of its basic critical flow rate equation upward by 20% for safety reasons, and the final Turner critical flow rate equation is shown in equation (17):

$$v_{cr} = 6.6 \left[\frac{\sigma(\rho_l - \rho_g)}{\rho_g^2} \right]^{0.25} \tag{17}$$

where σ is the gas-liquid interfacial tension, m/N; ρ_g is the gas density, m^3/kg; ρ_l is the liquid density, m^3/kg.

2.1.6 Critical solid-carrying model

The minimum gas flow rate for solid entrainment is equivalent to the terminal settling velocity of the particles. In vertical wells, solid particles initially accelerate downwards. When the resistive force exerted on the particles reaches a magnitude that counteracts the

disparity between gravitational pull and upward thrust, the particulate matter will commence descending at a steady rate. This velocity is referred to as the terminal settling velocity of the particles. The formula for particle settling velocity is shown in equations (18) and (19):

$$v_s = \sqrt{\frac{4gd_s\left(\rho_s - \rho_g\right)}{3\rho_g C_D}}\frac{\psi}{1+d_s/D_h} \tag{18}$$

$$Re_s = \frac{\rho_s v_s d_s}{\mu} \tag{19}$$

where v_s is the particle settling velocity, equal to the solid-carrying critical flow rate, m/s; d_s is the equivalent diameter of particles, m; D_h is the equivalent diameter of wellbore, m; ρ_s is the solid phase particle density, kg/m^3; Ψ is the sphericity, dimensionless; Re_s is the Reynolds number of particles; C_D is the drag coefficient, dimensionless; laminar flow region $C_D = 24/Re_s$, transition region $C_D = 10/\sqrt{Re_s}$, Turbulent flow region $C_D = 0.45$; μ is the viscosity of sand flushing fluid, Pa·s.

2.1.7 Hydrate phase equilibrium model

To streamline the modelling process, the influence of natural gas composition is disregarded, with the assumption that the produced gas consists solely of methane. The methane hydrate phase equilibrium model established by Dzyuba and Zektser (2013), which is based on experimental data and takes into account only temperature and pressure, is shown in equation (20).

$$T_m = 9.6330 \ln p_{eq} + 264.9661 \tag{20}$$

where p_{eq} is the hydrate phase equilibrium pressure, MPa.

2.2 Model verification

To assess the validity of the developed simulation, an experiment was conducted using a 30 m high, 76.2 mm inner diameter visible acrylic tube (Figure 3). In the selection of foaming agents, foaming agents are mainly categorised into four types: anionic, cationic, amphoteric, and non-ionic foaming agents. Among them, the UT and CT series are commonly used in field applications. Shi and Wang (2016) conducted experimental evaluations of the foaming agents currently used in the field and found that UT-4 is the most suitable under conditions where the temperature is below 60°C and no condensate oil is present. Yan's (2017) research indicated that a foaming agent concentration of 0.5% is optimal. Therefore, considering factors such as foaming ability, foam stability, and experimental temperature, a 0.5% UT-4 foam drainage agent was selected (Figure 4).

Some amount of foam, water, and 1 mm-diameter gravel were added to simulate the conditions of sand production and accumulated fluid at the wellbore bottom after hydrate extraction. With a fixed nitrogen injection rate of 70 m^3/h, experimental data were obtained, and a comparison curve was plotted between the calculated rheological parameters of the wellbore and the actual data. The experimental results and data analysis are shown in Figures 5 and 6.

Figure 3 Vertical pipe transport system (see online version for colours)

Figure 4 Foma for experiment (see online version for colours)

Figure 5 Experimental phenomenon of 70 m^3/h nitrogen inject rate and 1 mm particle size (see online version for colours)

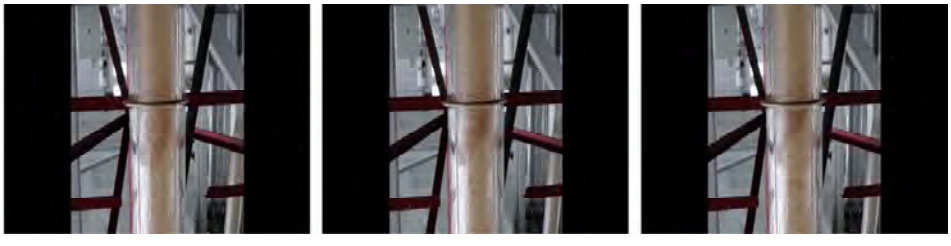

After calculating and analysing the two datasets, the comparison results are shown in Table 1. Both datasets fall within the acceptable error range, confirming the accuracy and reliability of the constructed mathematical model.

Figure 6 Comparison curves between theoretical and experimental values, (a) comparison curves of wellbore pressure and wellbore temperature (b) comparison curve of the velocity of each phase (c) comparison curves of each phase content (see online version for colours)

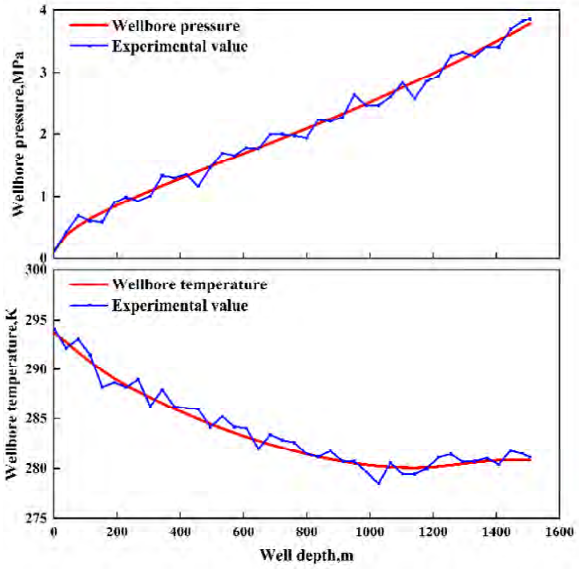

(a)

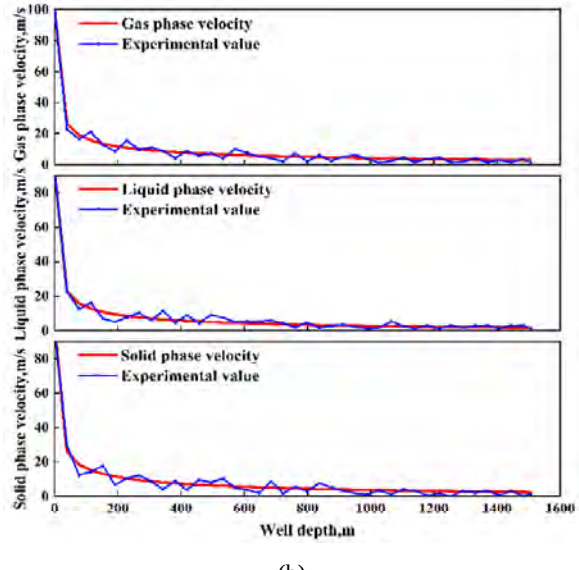

(b)

Figure 6 Comparison curves between theoretical and experimental values, (a) comparison curves of wellbore pressure and wellbore temperature (b) comparison curve of the velocity of each phase (c) comparison curves of each phase content (continued) (see online version for colours)

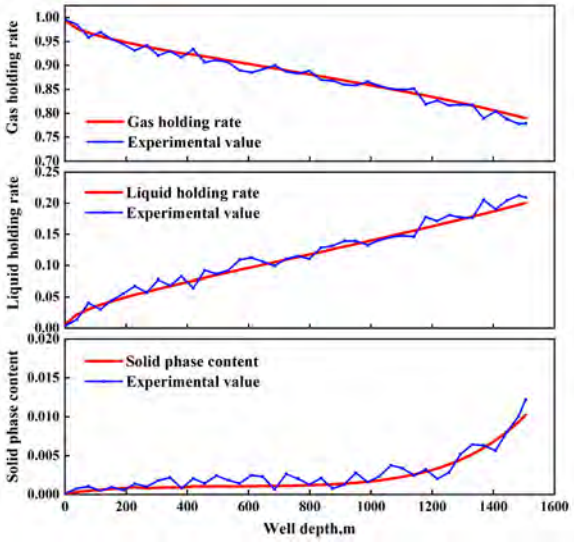

(c)

Table 1 Numerical comparisons and error table

	Calculated value	*Experimental value*		*Average error*
Wellbore pressure	3.79 MPa	3.86 MPa	Wellbore pressure	5.69%
Wellbore temperature	280.81 K	281.11 K	Wellbore temperature	6.58%
Minimum gas phase velocity	2.93 m/s	2.29 m/s	Gas phase velocity	3.52%
Minimum liquid phase velocity	2.25 m/s	1.49 m/s	Liquid phase velocity	3.69%
Minimum solid phase velocity	1.71 m/s	1.12 m/s	Solid phase velocity	3.83%
Minimum gas holding rate	78.96%	77.87%	Gas holding rate	4.02%
Maximum liquid holding rate	20.02%	20.91%	Liquid holding rate	5.34%
Maximum solid holding rate	1.02%	1.22%	Solid holding rate	7.16%

3 Analysis of factors affecting the effectiveness of foam drainage in the wellbore

To investigate the influence of various physical parameters on continuous production in a wellbore under foam drainage conditions, based on the actual production test data (Ye et al., 2020), and in conjunction with a mathematical theoretical model for multiphase flow in a continuously producing wellbore, numerical calculations were conducted under different conditions of foam injection volume (nitrogen injection rate), gas production

rate, foam viscosity, and foam gas-liquid ratio. The calculations took into account that under standard conditions, 1 m^3 hydrate can decompose into a maximum of 0.8 m^3 water and 164 m^3 methane gas. The wellbore depth is 1,505 m, with a water depth of 1,225 m, the height from the drill platform to the sea surface is 27 m, the tubing size is 177.8 mm, the diameter of the coiled tubing is 88.9 mm, and the temperature of the sea surface is 298.15 K. The specific technical schemes are presented in Table 2.

Table 2 Technical program

Number	*Nitrogen injection rate* m^3/min	*Gas production rate* m^3/d	*Foam viscosity mPa·s*	*Gas-liquid ratio*	*Water production rate* m^3/d	*Sand production rate* m^3/d	*Sediment particle size mm*
1	60	20,000	8	120:1	30	10	1
2	75						
3	90						
4	60	5,000	8	120:1			
5		10,000					
6		20,000					
16	60	20,000	4	120:1			
17			8				
18			12				
19	60	20,000	8	120:1			
20				140:1			
21				160:1			

3.1 Nitrogen injection rate

In the operational parameters of a gas production rate of 20,000 m^3/d, a foam viscosity of 8 mPa·s, a foam gas-to-liquid ratio of 120:1, a water production rate of 30 m^3/d, a sand production rate of 10 m^3/d, and a sediment particle size of 1 mm, the nitrogen injection rates were set at 60 m^3/min, 75 m^3/min, and 90 m^3/min, respectively. A simulation of foam circulation was performed to examine the fluctuations in wellbore pressure, wellbore temperature, liquid and solid carrying capacity under different nitrogen injection rates, as illustrated in Figure 7.

The graphical data demonstrate that during continuous foam drainage operations, as the rate of nitrogen injection escalates from 60 m^3/min to 90 m^3/min, the system's liquid and solid carrying capacities are enhanced due to the combined effects of changes in mixed fluid density and frictional pressure drop. Specifically, the minimum gas phase velocity increases from 2.71 m/s to 3.17 m/s, reflecting enhanced gas phase kinetic energy, which in turn promotes improvements in liquid-carrying and solid-carrying capacities. This variation leads to increases in the minimum liquid phase velocity and minimum solid phase velocity to 2.15 m/s and 1.50 m/s (from 1.37 m/s and 0.81 m/s, respectively), as well as an elevation in the minimum gas holdup (from 70.60% to

76.75%). Conversely, the maximum liquid holding rate and maximum solid content decrease to 22.15% and 1.10% (from 26.54% and 2.86%, respectively). Simultaneously, the bottomhole pressure rises from 3.50 MPa to 4.80 MPa, while the bottomhole temperature slightly increases to 281.21 K (from 280.75 K). From Figure 7(a), it can be seen that the temperature within the wellbore consistently exceeds the phase equilibrium temperature, so there is no hydrate formation.

Figure 7 The variation patterns under different nitrogen injection rates, (a) wellbore temperature and pressure (b) liquid and solid carrying capacity (c) content of each phase (d) velocity of each phase (see online version for colours)

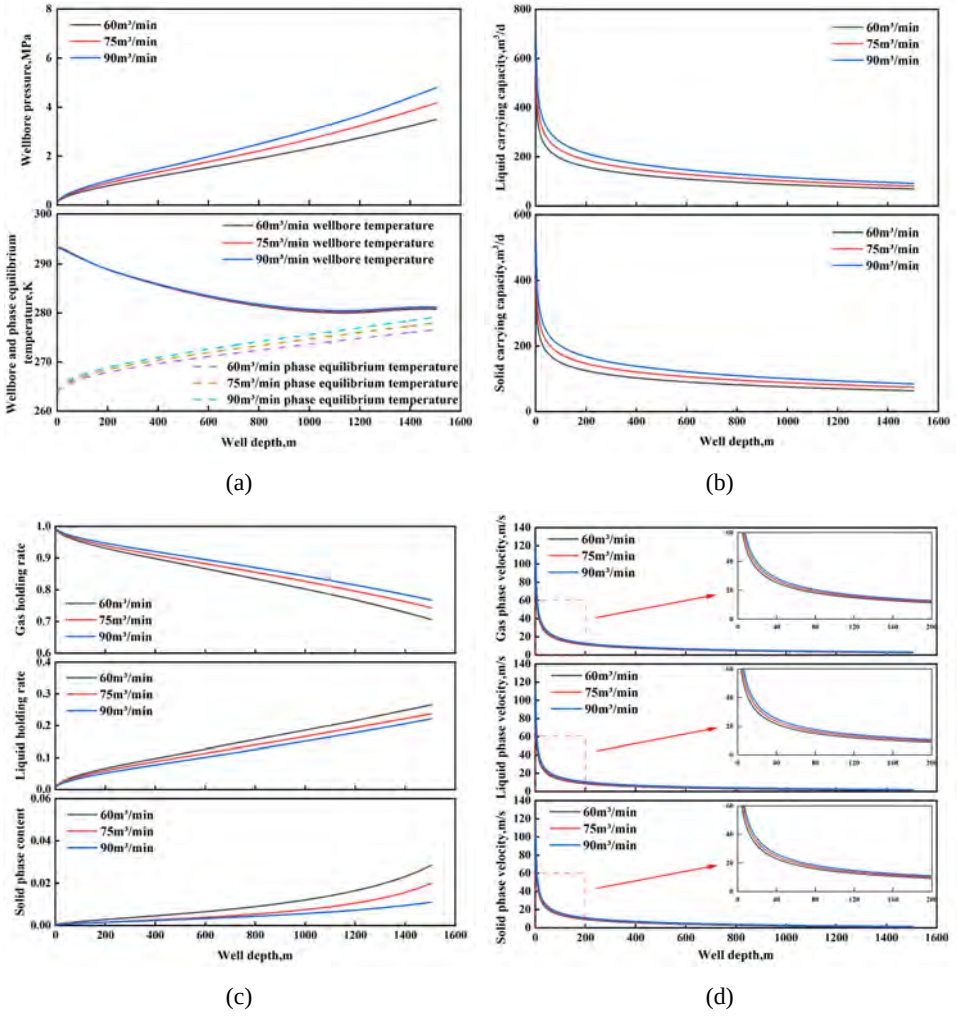

Based on the above analysis, in the foam drainage process, moderately increasing the nitrogen injection rate has a positive impact on achieving safe and efficient liquid and solid carrying operations. Specifically, the increase in nitrogen not only directly

contributes to the expansion of foam volume but also improves the stability of the foam system. The lower density of the foam provides favorable conditions for enhancing liquid and solid carrying efficiency, ensuring that the foam persists longer within the pipeline system and thus achieving continuous and effective carrying of liquids and solid particles. Additionally, the incorporation of nitrogen can effectively reduce the viscosity of the foam system, enhancing its fluidity within the pipeline and ensuring smooth transportation of the foam in complex pipeline environments. This reduces equipment failures or production interruptions caused by foam blockage or instability. Based on this analysis, in actual production operations, a relatively high level of nitrogen injection rate can be appropriately maintained to maximise the effectiveness and advantages of foam production technology.

3.2 Gas production rate

In the operational parameters of a nitrogen injection rate of 60 m^3/min, a liquid injection rate of 0.5 m^3/min, a foam gas-to-liquid ratio of 120:1, a foam viscosity of 8 mPa·s, a water production rate of 30 m^3/d, a sand production rate of 10 m^3/d, and a sediment particle size of 1 mm, the gas production rates were set at 5,000 m^3/d, 10,000 m^3/d, and 20,000 m^3/d, respectively. A simulation of foam circulation was performed to examine the fluctuations in wellbore pressure, wellbore temperature, liquid and solid carrying capacity under different gas production rates, as illustrated in Figure 8.

The graphical data illustrate that in continuous foam-drainage operations, as the daily gas production increased from 5,000 m^3/d to 20,000 m^3/d, the foam's capacity for transporting liquids and solids improved significantly. Specifically, the minimum gas velocity rose from 1.94 m/s to 2.61 m/s. The acceleration in gas velocity enhanced the liquid-carrying capacity, subsequently driving an increase in the liquid-phase velocity, with the minimum liquid velocity increasing from 0.97 m/s to 1.37 m/s. Similarly, the increase in gas velocity also strengthened the solid-carrying capacity, with the minimum solid-phase velocity rising from 0.37 m/s to 0.81 m/s. Consequently, as gas production increased, the minimum gas holding rate, maximum liquid holding rate, and maximum solid content changed to 75.00%, 22.14%, and 2.86%, respectively (from 68.82%, 26.39%, and 4.79%). Additionally, the bottomhole pressure decreased from 4.95 MPa to 3.50 MPa, while the bottomhole temperature increased from 279.74 K to 280.75 K. Under the calculated conditions, the wellbore temperature consistently remained above the hydrate phase equilibrium temperature, and there was no hydrate formation in the wellbore.

Therefore, in continuous foam-drainage operations, an increase in gas production exerts a positive influence on the liquid and solid carrying capacity. Specifically, as gas production rises, the foam exhibits more uniform flow behaviour within the wellbore, significantly enhancing the 'bubble-driven effect'. This allows bubbles to more effectively carry liquid and solid particles upward during their ascent, effectively reducing the accumulation of liquids and solids within the wellbore. Consequently, it mitigates the potential risks of liquid loading or blockage in the wellbore, ensuring the safety and efficiency of drainage operations.

Figure 8 The variation patterns under different gas production rates, (a) wellbore temperature and pressure (b) liquid and solid carrying capacity (c) content of each phase (d) velocity of each phase (see online version for colours)

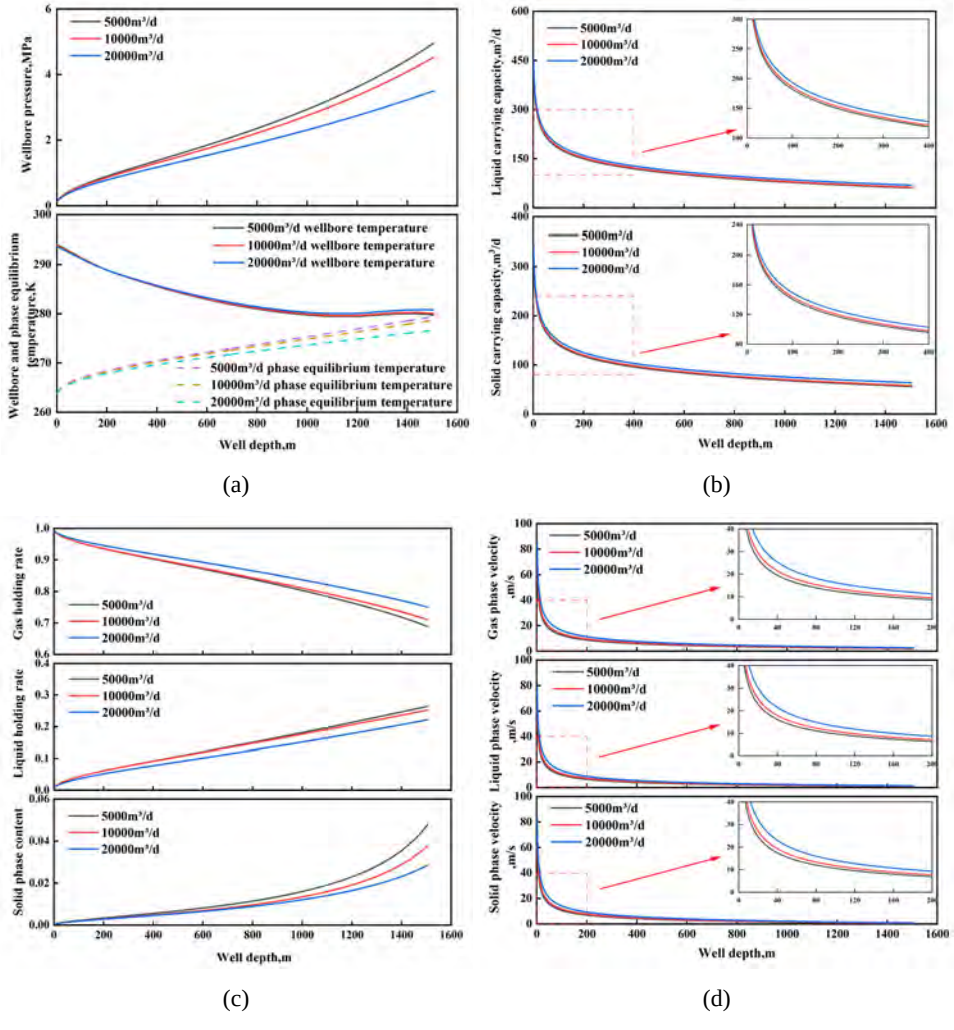

3.3 Foam viscosity

In the operational parameters of a nitrogen injection rate of 60 m^3/min, a liquid injection rate of 0.5 m^3/min, a foam gas-to-liquid ratio of 120:1, a gas production rate of 20,000 m^3/d, a water production rate of 30 m^3/d, a sand production rate of 10 m^3/d, and a sediment particle size of 1 mm, the foam viscosities were set at 4 mPa·s, 8 mPa·s and 12 mPa·s, respectively. A simulation of foam circulation was performed to examine the fluctuations in wellbore pressure, wellbore temperature, liquid and solid carrying capacity under different foam viscosities, as illustrated in Figure 9.

The graphical data indicate that as the foam viscosity increased from 4 mPa·s to 12 mPa·s, the foam's liquid and solid carrying capacity exhibited a declining trend. This

reduction is attributed to the dual effects of increased mixed fluid density and intensified frictional pressure drop. Specifically, the minimum gas velocity declined from 2.97 m/s to 2.31 m/s, which directly weakened the foam's liquid-carrying capacity, subsequently leading to a decline in both liquid and solid carrying capacity. As a result, the minimum liquid velocity and minimum solid velocity decreased to 1.47 m/s and 0.76 m/s, respectively (from 1.59 m/s and 0.87 m/s). Concurrently, the minimum gas holding rate dropped from 79.50% to 72.22%, while the maximum liquid holding rate and maximum solid phase content increased to 24.55% and 3.23%, respectively (from 18.29% and 2.21%). During this period, the wellbore pressure rose from 3.32 MPa to 4.56 MPa, and the bottomhole temperature increased from 279.79 K to 282.2 K.

Figure 9 The variation patterns under different foam viscosities, (a) wellbore temperature and pressure (b) liquid and solid carrying capacity (c) content of each phase (d) velocity of each phase (see online version for colours)

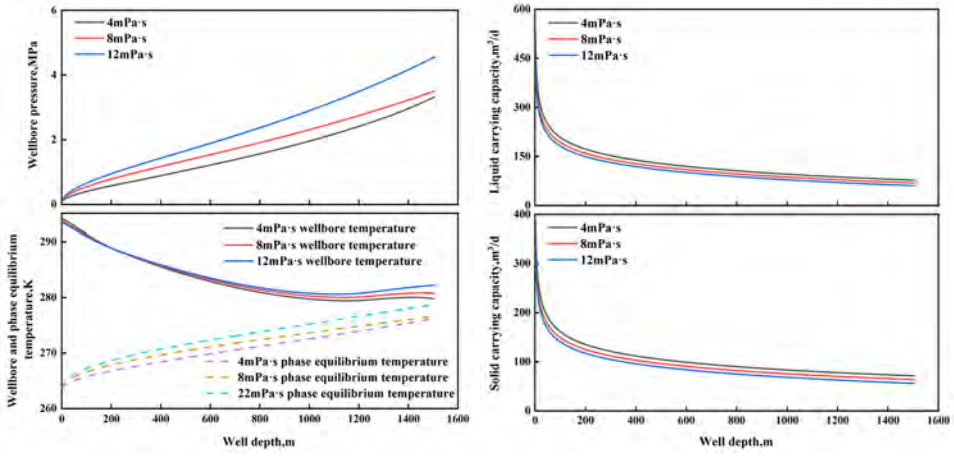

(a) (b)

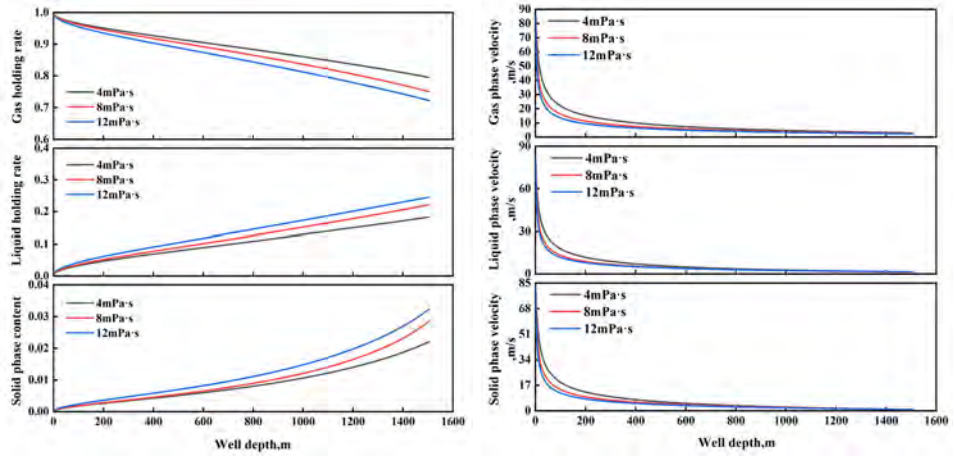

(c) (d)

Although a higher foam viscosity enhances foam stability, consider that foam primarily consists of highly compressible gas, pressure changes have a significant effect on its flow rate. The increase in foam viscosity amplifies the frictional pressure drop within the wellbore, leading to a reduction in flow velocity. Consequently, the liquid-carrying and sand-carrying capacities of the foam are diminished. However, it is noteworthy that excessively low foam viscosity may also compromise foam stability, making it prone to collapse, which can adversely affect drainage efficiency.

Figure 10 The variation patterns under different gas-liquid ratios, (a) wellbore temperature and pressure (b) liquid and solid carrying capacity (c) content of each phase (d) velocity of each phase (see online version for colours)

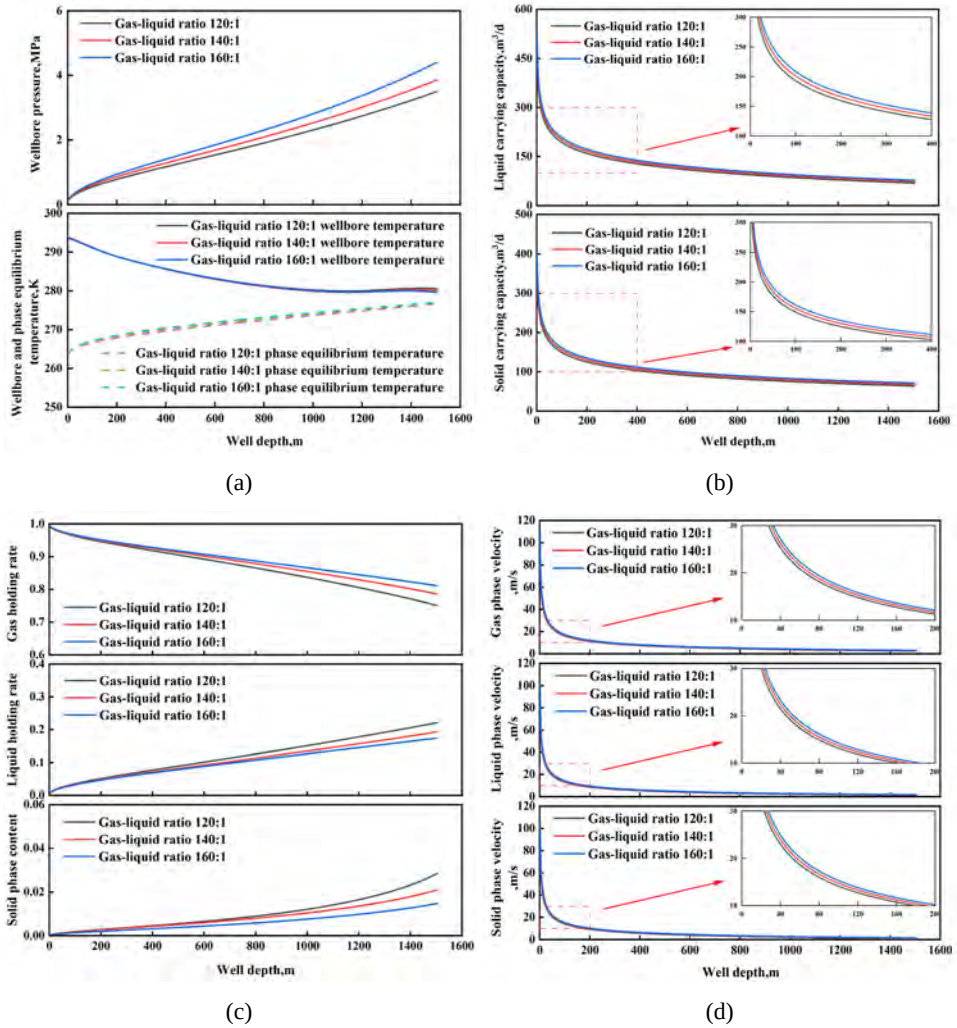

3.4 Gas-liquid ratio

In the operational parameters of a gas production rate of 20,000 m^3/d, a foam viscosity of 8 mPa·s, a water production rate of 30 m^3/d, a sand production rate of 10 m^3/d, and a sediment particle size of 1 mm, the liquid injection rate was maintained at 0.5 m^3/min. By setting the nitrogen injection rates at 60 m^3/min, 70 m^3/min, and 80 m^3/min, to achieve different gas-to-liquid ratios of 120:1, 140:1, and 160:1, respectively. A simulation of foam circulation was performed to examine the fluctuations in wellbore pressure, wellbore temperature, liquid and solid carrying capacity under different gas-liquid ratios, as illustrated in Figure 10.

The graphical data indicate that as the gas-liquid ratio of the foam increases, the system's ability to carry both liquid and solid phases improves. Specifically, the minimum gas velocity exhibits an increase from 2.50 m/s to 3.04 m/s, and this augmentation in gas velocity enhances the foam's capacity to carry both liquid and solid phases. Similarly, the minimum liquid velocity rises from 1.37 m/s to 1.81 m/s, while the minimum solid velocity increases from 0.81 m/s to 1.43 m/s. Correspondingly, there is an elevation in the minimum gas holding rate, from 75.00% to 81.08%, and the maximum liquid holding rate and the maximum solid phase content decrease to 17.45% and 1.47%, respectively (from 22.15% and 2.85%). Additionally, the bottomhole pressure increases from 3.50 MPa to 4.40 MPa, whereas the bottomhole temperature drops from 280.57 K to 279.6 K. The wellbore temperatures remain above the hydrate phase equilibrium temperature throughout.

Comprehensive analysis reveals that during continuous foam injection production, a higher foam gas-liquid ratio leads to smoother foam flow, reducing fluctuations that occur during single-phase gas or liquid flow, thereby ensuring the stability of continuous production. Simultaneously, the increase in bubble quantity results in a more uniform foam structure, with gas and liquid being evenly dispersed within the foam. This enhances the foam's ability to carry both liquid and solid phases. Under conditions of a higher gas-liquid ratio, the pressure distribution within the foam becomes more uniform, effectively inhibiting gas reflux and avoiding the issue of reverse gas flow within the wellbore during the production process. Therefore, a higher foam gas-liquid ratio not only prevents the formation of hydrates but also facilitates safe liquid and solid carrying.

4 Optimisation of engineering parameters

Based on the first natural gas hydrate production test in the South China Sea, optimise the design of the engineering parameters of the vertical wellbore multiphase flow continuous discharge mining under the situation of sand out of the bottom of the well after the exploitation of the hydrate reservoir. The foundational parameters remain consistent with those presented in the previous section, and the specific calculation scheme is shown in Table 3.

4.1 Optimisation of engineering parameters under constant water production rate with different foam injection volumes

The variation patterns under different foam injection volumes at water production rates of 10 m^3/d, 30 m^3/d, and 50 m^3/d are illustrated in Figure 11.

Comparison of conditions with varying foam injection rates at a constant water production rate reveals the following trends: as the foam injection rate increases, influenced by mixed density and frictional pressure drop, the bottomhole pressure initially decreases and then increases; the bottomhole temperature undergoes minimal change; both the liquid and solid carrying capacity exhibit an upward turn; the minimum gas velocity, minimum liquid velocity, and minimum solid velocity all increase; the minimum gas-holding rate has been shown to increase, whilst the maximum liquid-holding rate and maximum solid-phase contents have both been found to decrease. On the other hand, comparison of conditions with a constant foam injection rate and varying water production rates shows the following: as the rate of water production escalates, both the bottomhole pressure and temperature increase; the minimum values of the velocity of each phase is decreasing; the minimum gas holding rate decreases, while the maximum liquid holding rate and maximum solid phase content increase.

Table 3 Numerical calculation and optimisation scheme for engineering parameters

Groups	*Water production rate*	*Foam injection rate*	*Solid production rate*	*Other identical operating conditions*
1	10 m^3/d	40 m^3/min	15 m^3/d	Gas production rate 20,000 m^3/d, solid phase particle size 1 mm, foam viscosity 8 mPa·s, liquid injection rate 0.5 m^3/min
2		60 m^3/min		
3		80 m^3/min		
4		100 m^3/min		
5		120 m^3/min		
6	30 m^3/d	40 m^3/min		
7		60 m^3/min		
8		80 m^3/min		
9		100 m^3/min		
10		120 m^3/min		
11	50 m^3/d	40 m^3/min		
12		60 m^3/min		
13		80 m^3/min		
14		100 m^3/min		
15		120 m^3/min		
16		40 m^3/min	30 m^3/d	
17		60 m^3/min		
18		80 m^3/min		
19		100 m^3/min		
20		120 m^3/min		
21		40 m^3/min	50 m^3/d	
22		60 m^3/min		
23		80 m^3/min		
24		100 m^3/min		
25		120 m^3/min		

An increase in foam injection rate leads to a continuous enhancement in both liquid-carrying and solid-carrying capacities. However, it has been demonstrated that

when the foam injection rate reaches a specific level, the decrement in maximum liquid holding rate and maximum solid phase content becomes extremely minimal. Consequently, any further augmentation in the foam injection rate will yield only a marginal enhancement in the liquid and solid carrying capabilities. Consequently, for water production rates of 10 m^3/d, 30 m^3/d, and 50 m^3/d, it is recommended to employ a foam injection rate of 100 m^3/min.

Figure 11 The law of each parameter under certain water production and different foam injection volumes, (a) the variation patterns of wellbore pressure and bottomhole temperature (b) the variation patterns of minimum liquid and solid carrying capacities (c) the variation patterns of the minimum gas, liquid, and solid phase velocities (d) the variation patterns of the minimum gas holding rate, maximum liquid holding rate, and maximum solid phase content (see online version for colours)

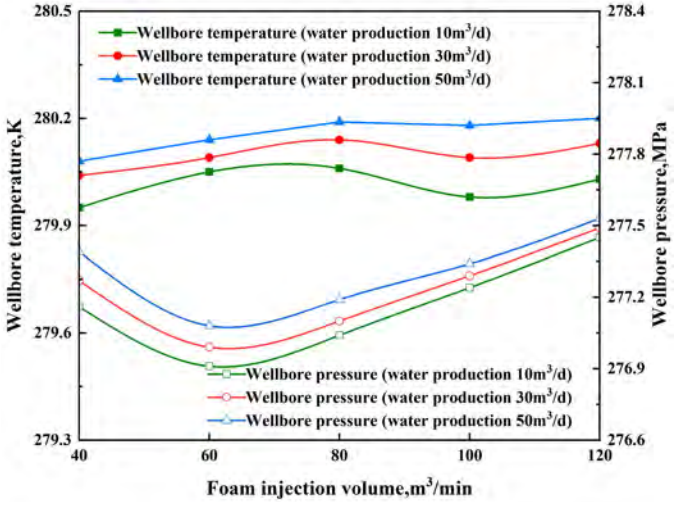

(a)

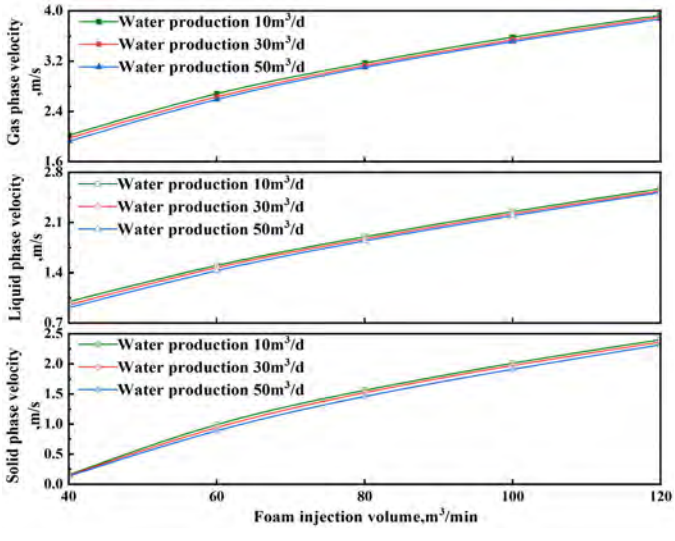

(b)

Figure 11 The law of each parameter under certain water production and different foam injection volumes, (a) the variation patterns of wellbore pressure and bottomhole temperature (b) the variation patterns of minimum liquid and solid carrying capacities (c) the variation patterns of the minimum gas, liquid, and solid phase velocities (d) the variation patterns of the minimum gas holding rate, maximum liquid holding rate, and maximum solid phase content (continued) (see online version for colours)

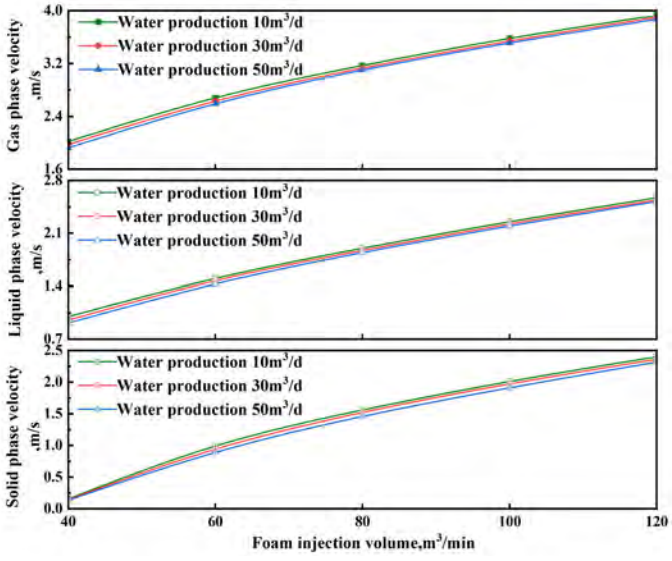

(c)

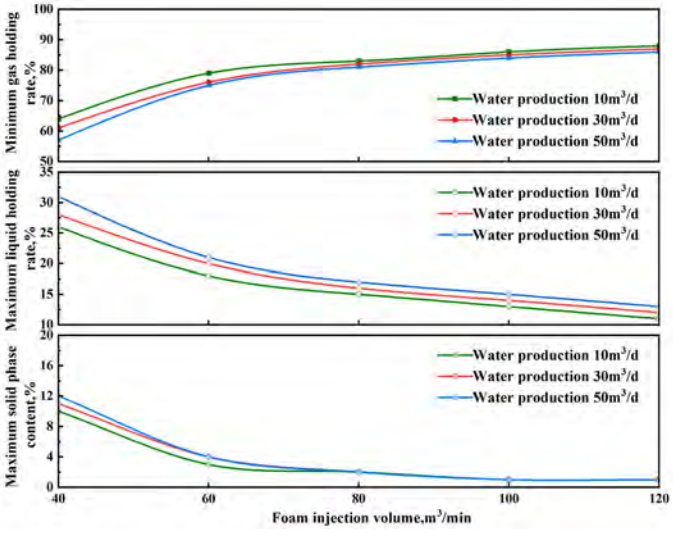

(d)

4.2 Optimisation of engineering parameters under constant sand production rate with different foam injection volumes

The variation patterns under different foam injection volumes at sand production rates of 15 m^3/d, 30 m^3/d, and 50 m^3/d are illustrated in Figure 12.

Figure 12 The law of each parameter under certain solid production and different foam injection volumes, (a) the variation patterns of wellbore pressure and bottomhole temperature (b) the variation patterns of minimum liquid and solid carrying capacities (c) the variation patterns of the minimum gas, liquid, and solid phase velocities (d) the variation patterns of the minimum gas holding rate, maximum liquid holding rate, and maximum solid phase content (see online version for colours)

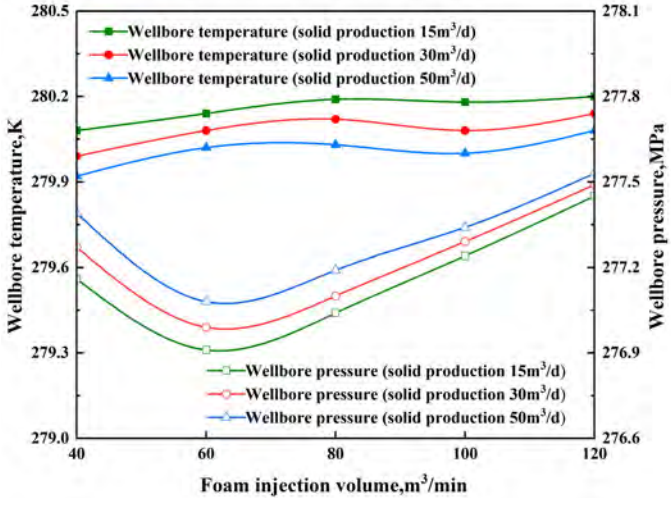

(a)

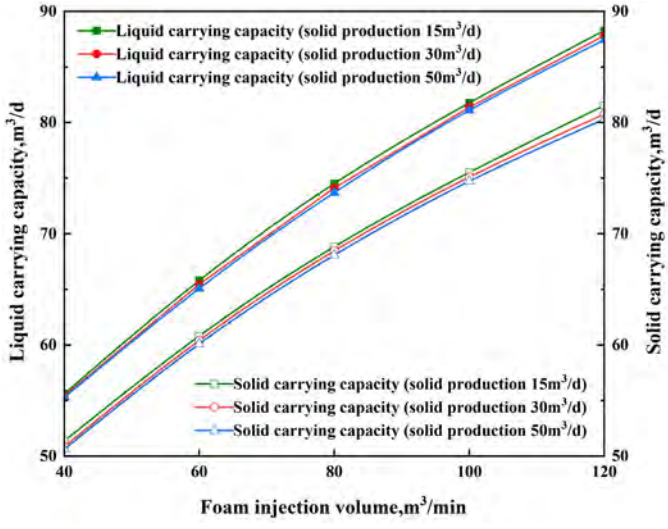

(b)

Figure 12 The law of each parameter under certain solid production and different foam injection volumes, (a) the variation patterns of wellbore pressure and bottomhole temperature (b) the variation patterns of minimum liquid and solid carrying capacities (c) the variation patterns of the minimum gas, liquid, and solid phase velocities (d) the variation patterns of the minimum gas holding rate, maximum liquid holding rate, and maximum solid phase content (continued) (see online version for colours)

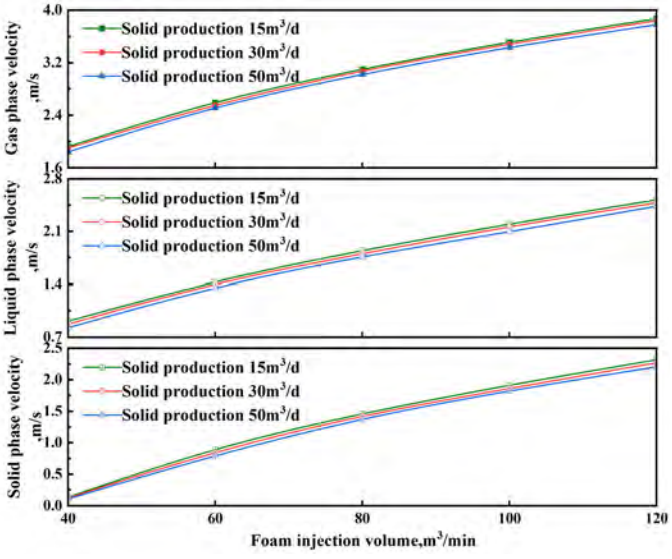

(c)

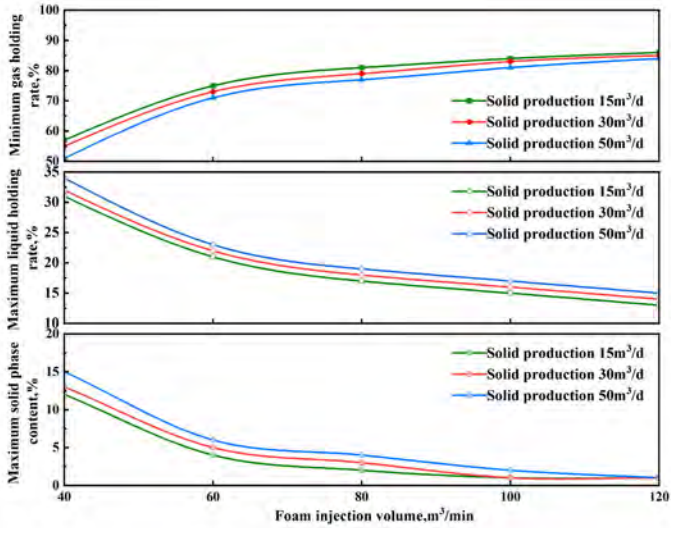

(d)

Under conditions with varying foam injection rates at a constant sand production rate, the variation patterns of the parameters of each phase are consistent with those observed under conditions of varying foam injection rates at a constant water production rate. Therefore, these patterns will not be elaborated upon here. As demonstrated in Figure

12(d), upon achieving a certain level of foam injection rate augmentation, the decline in maximum liquid holding rate and maximum solid phase content becomes negligible. Consequently, further augmentation of the foam injection rate will not yield substantial enhancement in liquid- and solid-carrying efficacy. Therefore, for sand production rates of 10 m^3/d, 30 m^3/d, and 50 m^3/d, the recommended foam injection rates are 100 m^3/min, 100 m^3/min, and 120 m^3/min, respectively.

5 Limitations of the study

In this study, only the drainage and sand removal performance under the same foam drainage agent was considered, without comparing the effects of different agents at varying concentrations. In addition, the analysis only considers the effects of individual variables on drainage and sand removal performance, without accounting for the interactions between different variables, resulting in a certain gap from real-world field applications.

Future research could focus more on the interactions among multiple variables and their combined effects on drainage and production efficiency. At the same time, current research remains limited to numerical simulations and laboratory experiments of continuous gas-water-sand-hydrate production under foam drainage conditions. In the future, more emphasis should be placed on research in engineering applications to enable early implementation in field operations.

6 Conclusions

This study addresses the issue of foam-assisted drainage in hydrate reservoirs following sand production. Utilising a multiphysics coupling approach, a numerical model for continuous foam drainage in wellbores was developed. The influences of nitrogen injection volume, gas production rate, foam viscosity, etc, were analysed to elucidate the sensitivity of continuous foam drainage performance under sand production conditions in hydrate reservoirs. Building upon this foundation and drawing insights from the first natural gas hydrate production test in the South China Sea, the engineering parameters for continuous multiphase flow drainage in vertical wellbores, under conditions of sand production following hydrate reservoir exploitation, were optimised. The principal conclusions derived from the research conducted in this study can be encapsulated as follows:

1 A theoretical mathematical framework for analysing multiphase flow within continuous drainage wellbores was established and verified for accuracy using experimental data. The average errors between the model predictions and experimental data were all within 8%, demonstrating the model's accuracy and reliability.

2 Under the same conditions, an increase in nitrogen injection rate helps expand the foam volume and improve the foam system's stability, thereby enhancing the system's ability to carry liquids and solids and improving foam drainage efficiency.

3 Under the same conditions, an increase in gas production rate favours a more uniform flow pattern of the foam in the wellbore, effectively reducing the accumulation of liquids and solids inside the wellbore, and ensuring the efficiency and safety of the drainage operation.

4 Under the same conditions, while an increase in foam viscosity helps improve foam stability, it has a more significant negative impact on flow velocity, resulting in a decline in the foam's capacity to transport both liquids and solids, which is detrimental to wellbore foam drainage. However, excessively low viscosity may also result in insufficient foam stability, causing the foam to easily break down, with similarly adverse effects.

5 Under the same conditions, an increase in the gas-liquid ratio of the foam leads to smoother foam flow and improves the uniformity of the foam structure, enhancing its ability to carry liquids and solids and improving foam drainage efficiency.

6 Based on the first natural gas hydrate production test in the South China Sea, engineering parameters were optimised for different water and sand production volumes. For water production rates of 10 m^3/d, 30 m^3/d, and 50 m^3/d, a foam injection rate of 100 m^3/min is recommended. For sand production rates of 10 m^3/d, 30 m^3/d, and 50 m^3/d, foam injection rates of 100 m^3/min, 100 m^3/min, and 120 m^3/min are recommended, respectively.

Declarations

This work was financially supported by National Natural Science Foundation of China (Number U2444216), National Key Laboratory of Marine Gas Hydrates Director Fund (2024) (Number CCL2024RCPS0275KQN), 111 Project (Number D21025), High-end Foreign Expert Introduction Program (Number G2021036005L), and National Key Research and Development Program (Number 2023YFC2811002, 2021YFC2800903).

All authors declare that they have no conflicts of interest.

Reference

Alooghareh, M.H., Kabipour, A., Ghazavi, M., Sisakht, S.M.M. and Razavifar, M. (2022) 'Effects of different gases on the performance of foams stabilized by cocamidopropyl betaine surfactant and silica nanoparticles: a comparative experimental study', *Petroleum*, Vol. 8, No. 4, pp.546–551, DOI: 10.1016/j.petlm.2021.09.002.

Alyousef, Z., Almobarky, M. and Schechter, D. (2018) 'The effect of nanoparticle aggregation on surfactant foam stability', *Journal of Colloid and Interface Science*, Vol. 511, pp.365–373, DOI: 10.1016/j.jcis.2017.09.051.

Boussa, M. (2004) 'Production optimization of gas wells: problem of water influx', Paper presented at the *SPE International Thermal Operations and Heavy Oil Symposium and Western Regional Meeting*, March, Bakersfield, California, DOI: 10.2118/86942-MS.

Dzyuba, A.V. and Zektser, I.S. (2013) 'Variations in submarine groundwater runoff as a possible cause of decomposition of marine methane-hydrates in the Artcic', *Water Resour.*, Vol. 40, pp.74–83, DOI: 134/S009780781301003X.

Etemad, S., Kantzas, A. and Bryant, S. (2022) 'A systematic analysis of foam drainage: experiment and model', *Results in Engineering*, Vol. 15, DOI: 10.1016/j.rineng.2022.100551.

Fu, Q., Zhou, S.W. and Li, Q.P. (2015) 'Natural gas hydrate exploration and production technology research status and development strategy', *Engineering Science*, Vol. 17, No. 9, pp.123–132, DOI: 10.3969/j.issn.1009-1742.2015.09.020.

Fujii, T., Noguchi, S., Takayama, T., Suzuki, K., Yamamoto, K. and Saeki, T. (2013) 'Site selection and formation evaluation at the 1st offshore methane hydrate production test site in the Eastern Nankai Trough, Japan', *Journal of Sociolinguistics*, Vol. 8, No. 8, pp.408–432, DOI: 10.3997/2214-4609.20131159.

Guo, L., Liang, J., Wang, R.Y., Luo, K., Jiang, Y.X. and Song, Y. (2023) 'Cloud-based monitoring system for foam content at the wellhead of foam drainage gas production', *IEEE Sensors Journal*, Vol. 23, No. 9, pp.9952–9958, DOI: 10.1109/JSEN.2023.3262395.

Haberer, R.M., Mangelsdorf, K., Wilkes, H. and Horsfield, B. (2006) 'Occurrence and palaeoenvironmental significance of aromatic hydrocarbon biomarkers in oligocene sediments from the Mallik 5L-38 gas hydrate production research well (Canada)', *Organic Geochemistry*, Vol. 37, No. 5, pp.19–538, DOI: 10.1016/j.orggeochem.2006.01.004.

Hou, M.F., Pan, S.Q. and Liu, H.L. (2021) 'World energy trend and China's oil and gas sustainable development strategies', *Natural Gas Industry*, Vol. 41, No. 12, pp.9–16, DOI: 10.3787/j.issn.1000-0976.2021.12.002.

Jin, M., Wang, Q., Liang, L. and Tan, J. K, (2024) 'Effect of particles on foam drainage', *Minerals Engineering*, Vol. 210, DOI: 10.1016/j.mineng.2024.108670.

Koehler, S.A., Stone, H.A. and Hilgfnfeldt, S. (2000) 'A generalized view of foam drainage: experiment and theory', *Langmuir: The ACS Journal of Surfaces and Colloids*, Vol. 16, No. 15, pp.6327–6341, DOI: 10.1021/LA9913147.

Kruglyakov, P.M., Karakashev, S.I., Nguyen, A.V. and Vilkova, N.G. (2008) 'Foam drainage', *Current Opinion in Colloid & Interface Science*, Vol. 13, No. 3, pp.163–170, DOI: 10.1016/j.cocis.2007.11.003.

Kurihara, M. (2005) 'Mallik 2002 gas hydrate production research well program: numerical simulation studies for analyzing the mechanism of gas production from methane hydrate reservoirs', *Journal of the Japan Institute of Energy*, Vol. 84, No. 2, pp.112–118.

Kurihara, M., Sato, A., Funatsu, K., Ouchi, H. and Ashford, D. (2010) 'Analysis of production data for 2007/2008 Mallik gas hydrate production tests in Canada', Paper presented at the *International Oil and Gas Conference and Exhibition in China*, June, Beijing, China, DOI: 10.2118/132155-MS.

Lai, N.J., He, Y.L., Zhang, X.C., Deng, J.W. and Wang, Z.X. (2023) 'Synthesis and performance evaluation of temperature and salt-resistant foam drainage agent XY-1', *Research Article – Chemical Engineering*, Vol. 48, pp.8911–8923, DOI: 10.1007/s13369-022-07531-9.

Lai, N.J., Zhang, C.B., Wang, J.Q., Tang, L. and Ye, Z.B. (2022) 'Effects of different gases on the molecular behavior of alkyl glycosides at gas/liquid interface and foam stability', *Chemistry Select*, Vol. 7, No. 47, DOI: 10.1002/slct.202203090.

Li, J, Wen, M., Lei, L., Fu, C. and Jiang, Z.Y. (2024) 'Development and analysis of pH-sensitive surfactants for enhancing foam drainage gas retrieval', *Journal of Molecular Liquids*, Vol. 396, DOI: 10.1016/j.molliq.2024.124106.

Li, N., Jiang, W.D., Jiang, Y.X., Yang, J.M., Cao, G.Q. and Zheng, R. et al. (2023) 'Study into impacts of formation sands on foam performance during drainage gas production – take Qinghai Oilfield's Sebei Gasfield for example', *Frontiers in Earth Science*, Vol. 11, DOI: 10.3389/feart.2023.1180501.

Li, Q.P., Zhou, S.W., Zhao, J.F., Song, Y.C. and Zhu, J.L. (2022) 'Research status and prospects of natural gas hydrate exploitation technology', *Strategic Study of CAE*, Vol. 24, No. 3, pp.214–224, DOI: 10.15302/J-SSCAE-2022.03.022.

Li, Z.H., Zhao, Y., Lou, Y.S., Li, Z., Fang, M.Z. and Wei, C.Y. (2019) 'Changing laws of wellbore temperature during offshore deepwater well drilling', *Natural Gas Industry*, Vol. 39, No. 10, pp.88–94.

Ning, F.Z., Li, Z., Li, J.L., Zhang, X.C., Gu, S.X. and Feng, M.X. et al. (2024) 'Cold- and high-temperature-resistant bubbling agent suitable for Xushen gas field', *Oilfield Chemistry*, Vol. 41, No. 2, pp.322–328, DOI: 10.19346/j.cnki.1000-4092.2024.02.019.

Rahman, A., Shirif, E. and Torabi, F. (2024) 'Nanoparticle-stabilized CO2 foam flooding for enhanced heavy oil recovery: a micro-optical analysis', *Petroleum*, Vol. 10, No. 4, pp.696–704, DOI: 10.1016/j.petlm.2024.06.002.

Rahman, A., Torabi, F. and Shirif, E. (2023) 'Surfactant and nanoparticle synergy: towards improved foam stability', *Petroleum*, Vol. 9, No. 2, pp.255–264, DOI: 10.1016/j.petlm. 2023.02.002.

Shaibu, R., Sambo, C., Guo, B. and Dudun, A. (2021) 'An assessment of methane gas production from natural gashydrates: challenges, technology and market outlook', *Advances in Geo-Energy Research*, Vol. 5, No. 3, pp.318–332, DOI: 10.46690/ager.2021.03.07.

Shi, Y.C. and Wang, M.F. (2016) 'Evaluation of the performance of commonly used gas well soaking agents', *Chemical Management*, No. 36, p.48.

Silin, M.A., Magadova, L.A., Malyutin, S.A., Malkin, N.R., Kirichenko, S.E. and Cherygova, M.A. et al. (2018) *Composition and Method for Preparing the Foam Converter in order to Remove Liquid from the Bottomhole of Gas Condensate Wells*, RU2642743C1.

Stevenson, P., Mantle, M.D., Sederman, A.J. and Gladden, L.F. (2007) 'Quantitative measurements of liquid holdup and drainage in foam using NMRI', *AIChE J.*, Vol. 53, No.2, pp.290–296, DOI: 10.1002/aic.11068.

Turner, R.G., Hubbard, M.G. and Dukler, A.E. (1969) 'Analysis and prediction of minimum flow rate for continuous removal of liquids from gas wells', *Journal of Petroleum Technology*, Vol. 21, No. 11, pp.1475–1482, DOI: 10.2118/2198-PA.

Wei, N., Jiang, L., Zhao, J.Z., Zhou, S.W., Zhang, L.H. and Li, Q.P. et al. (2020) 'Prediction of the risk of non-equilibrium generation of gas hydrates in wellbores of marine gas-water co-production wells', *Natural Gas Industry*, Vol. 40, No. 7, pp.65–75.

Wei, N., Sun, W.T., Meng, Y.F., Zhou, S.W., Fu, Q. and Guo, P. et al. (2017) 'Annular phase behavior analysis during marine natural gas hydrate reservoir drilling', *Acta Petrolei Sinica*, Vol. 38, No. 6, pp.710–720.

Wu, Q.B. and Guo, D.H. (2023) 'Preparation and performance of betaine composite corrosion inhibition foaming agent', *Contemporary Chemical Industry*, Vol. 43, No. 02, pp.186–190, DOI: 10.16606/j.cnki.issn0253-4320.2023.02.035.

Xu, M. (2022) *Morphology Characterization and Mechanism of Formation Microscopic Sand Production during Gas Hydrate Dissociation*, MA thesis, China University of Geosciences, Beijing, China, DOI: 10.27492/d.cnki.gzdzu.2022.000283.

Yamamoto, K., Terao, Y., Fujii, T., Terumichi, I. and Kanno, T. (2014) 'Operational overview of the first offshore production test of methane hydrates in the Eastern Nankai Trough', Paper presented at the *Offshore Technology Conference*, May, Houston, Texas, DOI: 10.4043/ 25243-MS.

Yan, P. (2017) *The Preparation of Amphoteric Foam Drainage Agent for Gas Well and Its Laboratory Evaluation*, MA thesis, Shaanxi University of Science & Technology, Shaanxi, China.

Ye, J.L., Qin, X.W., Xie, W.W., Lu, H.L., Ma, B.J. and Qiu, H.J. et al. (2020) 'Major progress of the second trial mining of natural gas hydrate in the South China Sea', *Geology in China*, Vol. 47, No. 03, pp.557–568.

Zhang, A.Y., Wei, N., Cai, M., Li, H.T., Zhao, J.Z. and Zhang, L.H. et al. (2024) 'Assessment of forecasting hydrate blockage in foam drainage gas recovery wellbore', *Energy Sci. Eng.*, Vol. 12, pp.2770–2784, DOI: 10.1002/ese3.1749.

Zhao, J., Zheng, J.N., Wang, X.R., Dong, S., Yang, M.J. and Song, Y.C. (2022) 'Effects of underlying gas on formation and gas production of methane hydrate in muddy low-permeability cores', *Fuel*, Vol. 309, DOI: 309: 122128, 10.1016/j.fuel.2021.122128.

Zhu, G.T. (2020) *Research on Drainage and Gas Recovery Technology for Offshore Low-Yielding Gas Wells*, MA thesis, China University of Petroleum (East China), Shandong, China, DOI: 10.27644/d.cnki.gsydu.2020.002029.s